Sustainable Power Sources Based on High Efficiency Thermopower Wave Devices

SCHOLARONE™
Manuscripts

Sustainable Power Sources Based on High Efficiency Thermopower Wave Devices

Sayalee G. Mahajan[1,‡], Albert Tianxiang Liu[1,‡], Anton L. Cottrill[1], Yuichiro Kunai[1], David Bender[1], Javier Castillo Jr[1], Stephen L. Gibbs[1], and Michael S. Strano[1*]

[1] 77 Massachusetts Ave, Department of Chemical Engineering, Massachusetts Institute of Technology, Cambridge, MA, USA

[‡] These authors contributed equally to this work.

[*] Corresponding author's email address: strano@MIT.edu

Abstract

There is a pressing need to find alternatives to portable power sources such as Li-ion batteries, which contain toxic metals, present recycling difficulties due to harmful inorganic components, and rely on elements in finite global supply. Thermopower wave (TPW) devices, which convert chemical to electrical energy by means of self-propagating reaction waves guided along nanostructured thermal conduits, have the potential to address this demand. Herein, we demonstrate orders of magnitude higher chemical-to-electrical conversion efficiency of thermopower wave devices, in excess of 1%, with sustainable fuels such as sucrose and NaN_3 for the first time, that produce energy densities on par with Li-ion batteries operating at 80% efficiency (0.2 MJ/L versus 0.8 MJ/L). We show that efficiency can be increased significantly by selecting fuels such as sodium azide or sucrose with potassium nitrate to offset the inherent penalty in chemical potential imposed by strongly p-doping fuels, a validation of the predictions of Excess Thermopower theory. Such TPW devices can be scaled to lengths greater than 10 cm

Sustainable Power Sources Based on High Efficiency Thermopower Wave Devices

and durations longer than 10s, an over 5-fold improvement over the highest reported values, and they are capable of powering a commercial LED device. Lastly, a mathematical model of wave propagation, coupling thermal and electron transport with energy losses, is presented to describe the dynamics of power generation, explaining why both unipolar and bipolar waveforms can be observed. These results represent a significant advancement toward realizing TPW devices as new portable, high power density energy sources that are metal-free.

Introduction

Current battery technology is typically comprised of toxic metals, presenting problems for recycle, and environmental exposure.[1] There is a pressing need for portable power sources that are sustainable, preferably using materials that are not in finite supply or mined from the earth, such as lithium.[2] Over the past decade, researchers have explored many potential alternatives, namely secondary batteries made with other metals,[2-5] pure organic materials,[6] graphitic carbon nitride,[7] and even exotic bio-organic materials like DNA for energy conversion and storage.[8] Numerous reports have given high merits for nanotechnologies (i.e. functionalized graphene[9] and strongly coupled inorganic-nano-carbon hybrid materials[10]) in this field. Such approaches benefit from their use of metal free, organic materials, but have not yet demonstrated power or energy densities commensurate with power sources such as the Li-ion battery, at any size or time scale. The scaling with electrode area fundamentally limits specific power and energy output. Thermopower waves are a potential solution because the approach uses a self-propagating reaction wave to control the duration of energy release, accessing high power densities from simple, chemical fuels. First reported in 2010, thermopower waves convert chemical energy in the form of an adsorbed fuel directly to electrical current by means of self-propagating reaction waves guided along nanostructured thermal conduits. Such TPW devices have been shown to

Sustainable Power Sources Based on High Efficiency Thermopower Wave Devices

exhibit high power density comparable to that of Li-ion batteries (80,000 $\mu W/mm^3$ versus about 10,000 $\mu W/mm^3$ demonstrated for Li microbattery).[11] The high power and energy densities of such devices provide attractive scaling for Micro-Electro-Mechanical Systems (MEMS),[12] smart dust applications,[13] or wireless sensor network nodes.[14] Conduit types have included multi-walled carbon nanotubes (MWNTs);[11] single-walled carbon nanotubes (SWNT);[15] SWNT yarns; ZnO;[16,17] Bi_2Te_3 coated on alumina and terracotta;[18,19] Sb_2Te_3 coated on alumina, terracotta and MWNTs;[19,20] and MnO_2 coated alumina[21]. Fuels employed for TPW studies, on the other hand, have included 2, 4, 6-Trinitroaniline (TNA), picramide and nitrocellulose (with sodium azide),[15,22] and nanothermites consisting of aluminum (Al) iron oxide (γ-Fe_2O_3).[23] However, the efficiency of energy conversion is an issue that has not been significantly addressed to date, and reported data have ranged from 10^{-6} to 10^{-3} %. In this work, we show that such efficiency limitations have been dominated by radiative losses, convective losses and fuel selections that necessarily set up a partially-cancelling thermopower wave, limiting power generation. Improved design and fuel complexation gives rise to devices that exceed efficiencies of 1 % for the first time, commensurate with experimental power source technologies.[24] These results are inspired by a mathematical wave model that allows one to describe the transient voltage profile of the traveling thermal wave, capturing many important aspects of the wave dynamics. In many ways, this conceptual advance allows us to push the boundaries of the future portable power sources comprised of carbon nanomaterials, which challenges the current state of the art from both an energy and a sustainability point of view.

Main Text

Electrical power generation with the propagation of the concomitant reaction wave is described by the theory of excess thermopower, which describes the induced voltage as the sum of two

Sustainable Power Sources Based on High Efficiency Thermopower Wave Devices

distinct sources, namely thermoelectricity and the transient chemical potential gradient. The

former is driven by the temperature difference existing across the thermal conduit, while the

latter arises because of the chemical potential difference existing across the conduit.[25]

$$\Delta V_{TPW} = S\left(T_{back} - T_{front}\right) - \frac{1}{e}\left(\mu_{back} - \mu_{front}\right) \tag{1}$$

Here, S is the Seebeck coefficient of the device; T is the temperature; μ is the chemical potential

of the dominant charge carriers in the system, holes or electrons, and the subscript *front* and *back*

denotes the spatial frontend and backend of the SWNT conduit, respectively. One can then

define a chemical-to-electrical conversion efficiency (η) as the ratio of the output electrical

energy to the input chemical energy into the system:

$$\eta = \frac{\text{Output Electrical Energy}}{\text{Input Chemical Energy}} = \frac{\int_{t_{start}}^{t_{end}} \frac{\Delta V_{out}^{2}}{R_{ext}} dt}{m_{fuel}\left(-\Delta H_{rxn}\right)} \tag{2}$$

Here, t is the time coordinate, with the subscript indicating the start and end of the experiment;

m_{fuel} is the mass of the chemical fuel used and ΔH_{rxn} represents its specific heat of reaction. The

value of η does not include the initiation energy as it is generally orders of magnitude smaller

than the denominator in equation (2). Historically η has not exceeded approximately $10^{-3}\%$ in the

literature, primarily due to limitations in fuel coupling[25] (as shown below), radiative and

convective losses. Figure 1a shows a circuit diagram of a TPW device as a source producing an

open circuit voltage ΔV_{OC} with an internal resistance R_{int} which produces an output voltage ΔV_{out}

over an external resistance R_{ext}.[26] Figure 1b shows a typical (bipolar) voltage output obtained

from a nitrocellulose-SWNT yarn TPW device. One consequence of the excess thermopower

theory represented in equation (1) is that the additive chemical potential contribution, which is a

Sustainable Power Sources Based on High Efficiency Thermopower Wave Devices

fuel property, resulting significant variance in the $\Delta\mu$ contribution. Different fuels also change the adiabatic reaction temperature, affecting the first term in equation (1) as well.[27] A screening of potential fuels produced two of notable interest, namely sodium azide (NaN_3) and a carbohydrate fuel in the form of sucrose with a premixed oxidizer, potassium nitrate (KNO_3). We observed that these fuels led to a substantially improved efficiency as compared to a standard nitrocellulose fuel (Figure 1c). Up to 100 times improvement was observed for NaN_3 despite the fact that at 320 J gm^{-1} it has a heat of combustion $1/10^{th}$ of nitrocellulose (4200 J gm^{-1}).[28] Sucrose with KNO_3 dissolved in water at 35:65 ratio also consistently demonstrated more than a factor of 10 higher efficiency, despite having a similar heat of combustion to nitrocellulose.

With a decreased heat of combustion (therefore a reduced contribution from the thermoelectric effect), the amplified output electrical energy is accounted for by the enhanced excess thermopower ($\Delta\mu$ contribution) led by the favorable chemical doping.[25] To further investigate the effect of doping on the SWNT by the different chemical fuels tested, Raman spectroscopy analyses were performed (Figure 1d) where the G peak Raman shifts were converted to Fermi energies using the data reported by Farhat *et al.* and a method outlined in Abrahamson *et al.* (modified below).[25,29,30] With the presence of nitro groups, the electron withdrawing nitrocellulose is known to p-dope graphene and SWNT.[25] With this insight, we calculate a Fermi energy of -0.21 eV for the bare SWNT (1577 cm^{-1}) (known to be p-doped by O_2), and -0.28 eV for the nitrocellulose/NaN_3 doped SWNT (1584 cm^{-1}). As was found from model regression of experimental data (below). This p-doping by chemical fuel actually generates an opposing electronic wave, reducing efficiency. It is noteworthy that with a Raman shift around 1579 cm^{-1}, NaN_3 and sucrose/KNO_3 either lower the p-doping losses (-0.23eV) or supportively n-dope (+0.40 eV) the SWNT as compared with nitrocellulose/NaN_3. In either case, the Fermi level

Sustainable Power Sources Based on High Efficiency Thermopower Wave Devices

difference (and hence the chemical potential gradient) of at least 0.05 eV between the doped states of SWNT justifies the higher electrical energy output observed for using solely NaN_3 or sucrose/KNO_3 as chemical fuels. This link between fuel properties and efficiency, supported by the excess thermopower theory, promises further improvements in fuel design for TPW devices.

It is also noted that the temperatures of propagating TPW wavefronts can approach the adiabatic limit (2427 K for nitrocellulose) leading to substantial heat losses from the device. We find that suspending TPW devices within an airgap flanked by two parallel Bi_2Te_3 thermoelectric (TE) harvesters is effective for capture of radiative and convective energy losses (Figure 1e). Combined with fuels such as sucrose-KNO_3 and NaN_3, efficiencies in excess of 1 % can be achieved in this configuration (Figure 1f). This scheme necessarily generates more electrical energy than conventional thermophotovoltaic or combustion schemes by adding the high power density TPW.[31,32] There does not appear to be a correlation between adiabatic reaction temperature (760 K for NaN_3 and 1043K for sucrose/KNO_3) and efficiency, an indication that TPW devices are generally not limited by the conventional thermoelectric term, and operate distinctly from thermophotovoltaics.[24]

Reaction waves such as TPWs are theoretically solitons with highly nonlinear properties arising from the exponential thermal source term associated with reaction. This exponential term partially cancels any dissipation that would be observed from thermal diffusion, predicting infinite propagation along an infinite conduit. To test this empirically, we generated TPW devices of increasing length. Sample voltage outputs from NaN_3-based and sucrose/KNO_3-based TPW devices are shown in Figure 2a, displaying opposite polarity voltage pulses from opposing propagation directions, as expected. As seen from Figure 2b, the duration of energy generation scales linearly with length, and its wave propagation is captured in Figure 2c, with notable

Sustainable Power Sources Based on High Efficiency Thermopower Wave Devices

cooling behind the advancing wavefront. The discovery of the linear scaling of voltage duration versus device length suggests a potential route to the scaling-up of TPW devices. Indeed, with this knowledge in hand, we demonstrate the longest SWNT-based TPW device reported to date, both in terms of length (over 10 cm) and duration of energy generation (7 s). The wave propagation of said device is presented in Figure 2c, and this linear scaling of voltage duration to device length clearly goes beyond the limited length window investigated in the past (Figure 2d).

The results demonstrated in this work are a clear advance over the state of the art, and systems examined in the literature that have focused on conduit type. Figure 2e charts the increase in efficiency from approximately 10^{-6} % for SWNT-based devices in 2010 and subsequent increase as conventional TE materials were examined in the years following by other researchers.[15-23,33-35] While higher Seebeck coefficient conduit types do maximize the conventional thermoelectric term in equation (1),[18] this current work highlights the importance of the excess thermopower through constructive chemical doping toward increasing efficiency. Initially discovered by us, the use of nitrocellulose as a solid state fuel due to its high combustion enthalpy has been adopted by many researchers.[16,18,19,21,35] This work further reveals a criteria for selecting better performing fuels for TPW propagation, namely NaN_3 and sucrose/KNO_3, by taking advantage of their favorable electronic interactions with SWNTs. The observed increase in energy output by reducing the nitrocellulose level (as indicated by the decreased nitrocellulose/NaN_3 ratio in Figure 2f) can be attributed to both the enhanced maximum peak voltage, as well as the prolonged energy output duration. To clarify, our current work (Figure 2e, red) demonstrates the highest TPW device efficiencies to date with or without the use of external energy harvesting. These advances pave the way for future chemical fuel optimization through rational design for SWNT-based TPW or even broader applications. As a demonstration of a practical use of the

current high efficiency device, we use three NaN_3-fueled SWNTs connected in series with thermoelectric residual heat harvesters to charge a voltage step-up converter (Figure 2g). For the first time, we are able to reach 1.5 V, power and sustain a commercial light-emitting diode (LED) for over 20 s (Figure 2h), a practical milestone that promises additional gains in energy and power density.

Lastly, these observations are coupled to a detailed mechanistic model to provide insights on how conduit type, fuel and thermal losses contribute to energy and power density, as well as efficiency. Using the excess thermopower concept outlined in equation (1) as a starting point, this model is capable of describing the transient voltage output of TPW by simultaneously solving the heat and mass transport equations that govern the TPW propagation along the SWNT fiber. The transient temperature and mass profiles are then used to predict both terms in equation (1), including the time-dependent variation of doping levels as fuel reacts along the wavefront.[25] As shown previously, a 1D self-propagating TPW can be analyzed by studying the corresponding heat and mass transfer for a one-dimensional reaction system of continuous fuel layers.[36]

The system is initially at ambient temperature T_{amb}. The heat of reaction ($-\Delta H$) is assumed to be temperature invariant, with the reaction modeled as first order with an Arrhenius activation energy E_a and attempt frequency prefactor k_0. This formulation assumes a fast thermal equilibrium between the thermal conduit and the fuel layer.[36] The non-dimensional forms of the heat and mass balance equations are shown in equations (3) and (4), which can be solved using method of lines, with the space domain discretized as shown in Figure 3a.

Sustainable Power Sources Based on High Efficiency Thermopower Wave Devices

$$\frac{\partial u}{\partial \tau} = \frac{\partial^2 u}{\partial \xi^2} + y e^{-\frac{1}{u}} - w_{rad}\left(u^4 - u_{amb}^4\right) - w_{conv}\left(u - u_{amb}\right) \qquad (3)$$

$$\frac{dy}{d\tau} = -\beta y e^{-\frac{1}{u}} \qquad (4)$$

where u and y represent the non-dimensional temperature and fuel concentration, both of which are a function of the dimensionless space (ξ) and time (τ); w_{rad} and w_{conv} correspond to the dimensionless net radiative and convective heat transfer coefficients, respectively. Non-dimensionalization of variables also gives rise to an important factor β, the inverse dimensionless adiabatic temperature rise:[37]

$$\beta = \frac{C_{p,CNT} E_a}{\left(-\Delta H\right) R} \qquad (5)$$

where $C_{p,CNT}$ is the heat capacity of the SWNT conduit and R is the gas constant.

TPW devices can be modeled as voltage sources giving rise to a transient open circuit voltage difference (ΔV_{TPW}) across its ends, given in equation (1). When connected to an external electrical load or electrical resistance, we obtain useable output voltage (ΔV_{out}) and current flow through the load. If we can estimate the magnitude of the thermal gradient and the chemical potential gradient, for a system with a known Seebeck coefficient S, we can calculate the expected open circuit voltage (ΔV_{TPW}) for a given pair of fuel-thermal conduit TPW device. Using the values of the internal resistance of the TPW device (R_{int}) and the resistance of the load attached (R_{ext}), we can compute the expected output voltage (ΔV_{out}) as shown in Equation (6). In Figure 3b, we present a schematic of a circuit diagram for a TPW device with the expected voltage output.

Sustainable Power Sources Based on High Efficiency Thermopower Wave Devices

$$\Delta V_{out} = \frac{S\left(T_{back} - T_{front}\right) - \frac{1}{e}\left(\mu_{back} - \mu_{front}\right)}{1 + \frac{R_{int}}{R_{ext}}} \qquad (6)$$

This model allows us to gain intuitive understandings about the different trends observed in voltage output profiles.[38] From selected sample fits (SWNTs fueled with nitrocellulose), shown in Figure 4a-4f, it is clear that this model predicts the experimental results with fairly high accuracy and consistency. When the reaction wave undergoes complete propagation, we expect a double polarity thermoelectric voltage output contribution, where the voltage output peak after complete wave propagation is smaller in magnitude, such as what is seen in Figure 2b. The effect of excess thermopower will either boost or oppose the first of the double polarity peaks, depending on the sign of the Seebeck coefficient of the SWNT cluster and the type of doping induced by the fuel. When the thermoelectric and the excess thermopower voltage contributions oppose each other, the first peak which is ideally higher in magnitude (as compared to the reverse polarity second peak) is repressed, as shown in Figure 4c. In the case of partial propagation, we expect a single polarity thermoelectric voltage output (e.g. Figure 4f), since the reaction wave stops in the middle of the conduit and never reaches the other end to create the opposite temperature gradient. Again, depending on whether the effect of excess thermopower boosts or opposes the thermoelectric voltage output, one expects to see 'kinks' or multiple peaks in the single polarity peak voltage output. Examples of these situations can be found in Figure 4a, 4b, 4d, and 4e. The most interesting takeaway from these fits is that for the 20 nitrocellulose-SWNT TPW samples that were fitted, 17 samples show the effect of excess thermopower opposing the voltage output due to the thermoelectric effect. This finding agrees with the Raman results discussed earlier in Figure 1d, where we concluded that the p-doping nitrocellulose

Sustainable Power Sources Based on High Efficiency Thermopower Wave Devices

generates an excess thermopower voltage opposite to its thermoelectric counterpart, reducing the overall energy output of the nitrocellulose TPW devices. This qualitative agreement between our model and experimental Raman measurements strengthens our confidence in the current theoretical construct and its prospects in aiding further TPW device optimization.

In summary, on the basis of the theory of excess thermopower, the chemical to electrical conversion efficiency of thermopower wave devices was improved from 10^{-3} % to 10^{-2} % by using novel fuels such as NaN_3 and sucrose/KNO_3. Combining this improved performance of thermopower waves with external thermoelectric harvesting, we demonstrate a net energy conversion efficiency of up to 1 % and successfully illuminate an LED for 20 s. We propose a detailed 1D heat and mass transfer model to be used in combination with the theory of excess thermopower to explain the experimental voltage outputs from thermopower wave devices. The theoretical analyses for the voltage outputs from nitrocellulose-SWNTs, in combination with Raman spectroscopy and a variety of controlled experiments, suggest that choosing n-doping fuels might further boost the efficiency of these SWNT fiber-based thermopower wave devices.

References

1.   Melot, B. C., Tarascon, J. M. Design and preparation of materials for advanced electrochemical storage. *Accounts of Chemical Research* **46**, 1226–1238 (2013).
2.   Orikasa, Y. *et al.* High energy density rechargeable magnesium battery using earth-abundant and non-toxic elements. *Scientific Reports* **4**, 5622 (2014).
3.   McKerracher, R. D., Ponce de Leon, C., Wills, R. G. A., Shah, A. A., Walsh, F. C. A review of the Iron–Air secondary battery for energy storage. *ChemPlusChem* **80**, 323–335 (2015).

4. Zhao, X., Ma, L. Recent progress in hydrogen storage alloys for nickel/metal hydride secondary batteries. *International Journal of Hydrogen Energy* **34**, 4788–4796 (2009).
5. Kim, H. *et al.* Metallic anodes for next generation secondary batteries. *Chemical Society Reviews* **42**, 9011–9034 (2013).
6. Häupler, B., Wild, A., Schubert, U. S. Carbonyls: powerful organic materials for secondary batteries. *Advanced Energy Materials* **5**, (2015).
7. Gong, Y., Li, M., Wang, Y. Carbon nitride in energy conversion and storage: recent advances and future prospects. *ChemSusChem* **8**, 931–946 (2015).
8. Irimia-Vladu, M., Sariciftci, N. S., Bauer, S. Exotic materials for bio-organic electronics. *Journal of Materials Chemistry* **21**, 1350–1361 (2011).
9. Dai, L. Functionalization of graphene for efficient energy conversion and storage. *Accounts of Chemical Research* **46**, 31–42 (2013).
10. Wang, H., Dai, H. Strongly coupled inorganic-nano-carbon hybrid materials for energy storage. *Chemical Society Reviews* **42**, 3088–3113 (2013).
11. Choi, W., Abrahamson, J. T., Strano, J. M, Strano, M. S. Carbon nanotube-guided thermopower waves. *Materials Today* **13**, 22–33 (2010).
12. Walther, D. C., Ahn, J. Advances and challenges in the development of power-generation systems at small scales. *Progress in Energy and Combustion Science* **37**, 583–610 (2011).
13. Sailor, M. J., Link, J. R. "Smart dust": nanostructured devices in a grain of sand. *Chemical Communications*, 1375–1383 (2005).
14. Roundy, S., Steingart, D., Frechette, L., Wright, P., Rabaey, J. in *Wireless Sensor Networks* Vol. 2920 *Lecture Notes in Computer Science* (eds Holger Karl, Adam Wolisz, & Andreas Willig) Ch. 1, 1–17 (Springer Berlin Heidelberg, 2004).
15. Abrahamson, J. T. *et al.* Synthesis and energy release of nitrobenzene-functionalized single-walled carbon nanotubes. *Chemistry of Materials* **23**, 4557–4562 (2011).
16. Walia, S. *et al.* ZnO based thermopower wave sources. *Chemical Communications* **48**, 7462–7464 (2012).
17. Lee, K. Y., Hwang, H., Choi, W. Advanced thermopower wave in novel ZnO nanostructures/fuel composite. *ACS Applied Materials & Interfaces* **6**, 15575–15582 (2014).
18. Walia, S. *et al.* Oscillatory thermopower waves based on Bi_2Te_3 Films. *Advanced Functional Materials* **21**, 2072–2079 (2011).
19. Walia, S. *et al.* Sb_2Te_3 and Bi_2Te_3 based thermopower wave sources. *Energy & Environmental Science* **4**, 3558–3564 (2011).
20. Hong, S. *et al.* Enhanced electrical potential of thermoelectric power waves by Sb_2Te_3-coated multiwalled carbon nanotube arrays. *The Journal of Physical Chemistry C* **117**, 913–917 (2013).
21. Walia, S. *et al.* MnO_2-Based thermopower wave sources with exceptionally large output voltages. *The Journal of Physical Chemistry C* **117**, 9137–9142 (2013).
22. Yeo, T. *et al.* Effects of chemical fuel composition on energy generation from thermopower waves. *Nanotechnology* **25**, 445403–445412 (2014).
23. Hong, S. *et al.* Surface thermochemical reaction control utilizing planar anisotropic thermal conduit. *Energy & Environmental Science* **4**, 2045–2049 (2011).
24. Lenert, A. *et al.* A nanophotonic solar thermophotovoltaic device. *Nat Nano* **9**, 126–130 (2014).
25. Abrahamson, J. T. *et al.* Excess thermopower and the theory of thermopower waves. *ACS Nano* **7**, 6533–6544 (2013).

Sustainable Power Sources Based on High Efficiency Thermopower Wave Devices

26. Johnson, D. H. Origins of the equivalent circuit concept: the current-source equivalent. *Proceedings of the IEEE* **91**, 817–821 (2003).

27. Abrahamson, J. T., Strano, M. S. Analytical solution to coupled chemical reaction and thermally diffusing systems: applicability to self-propagating thermopower waves. *The Journal of Physical Chemistry Letters* **1**, 3514–3519 (2010).

28. Kim, C., Thomas, S. W., Whitesides, G. M. Long-duration transmission of information with infofuses. *Angewandte Chemie International Edition* **49**, 4571–4575 (2010).

29. Farhat, H. *et al.* Phonon softening in individual metallic carbon nanotubes due to the Kohn anomaly. *Physical Review Letters* **99**, 145506–145509 (2007).

30. The (μ_{end} - μ_{start}) term in equation (1) corresponding to the chemical potential driving force of the excess thermopower is given by $\Delta\mu = \Delta E_F = p_m \times E_{F,m} + p_s \times E_{F,s}$, where ΔE_F is the Fermi level shift between the start and the end of the SWNT conduit, and p_m and p_s are coefficients representing the fractions of metallic and semi-conductive SWNTs in unsorted fibers. Theses fractions are determined by the rolling vectors of the SWNTs, about 1/3 and 2/3, respectively, since the manufacturer uses a generic chemical vapor deposition process. Raman spectroscopy and the G peak frequency can be used to estimate the average Fermi level of electrons in the SWNT fiber quantitatively.

31. Datas, A., Algora, C. Development and experimental evaluation of a complete solar thermophotovoltaic system. *Progress in Photovoltaics: Research and Applications* **21**, 1025–1039 (2013).

32. Rephaeli, E., Fan, S. Absorber and emitter for solar thermo-photovoltaic systems to achieve efficiency exceeding the Shockley-Queisser limit. *Opt. Express* **17**, 15145–15159 (2009).

33. Choi, W. *et al.* Chemically driven carbon-nanotube-guided thermopower waves. *Nat Mater* **9**, 423–429 (2010).

34. Lee, K. Y., Hwang, H., Shin, D., Choi, W. Enhanced thermopower wave via nanowire bonding and grain boundary fusion in combustion of fuel/CuO-Cu$_2$O-Cu hybrid composites. *Journal of Materials Chemistry A* **3**, 5457–5466 (2015).

35. Hwang, H. *et al.* Investigation of the effect of the structure of large-area carbon nanotube/fuel composites on energy generation from thermopower waves. *Nanoscale Research Letters* **9**, 536–544 (2014).

36. Abrahamson, J. T. *et al.* Wavefront velocity oscillations of carbon-nanotube-guided thermopower waves: nanoscale alternating current sources. *ACS Nano* **5**, 367–375 (2010).

37. Mahajan, S. G. *et al.* Superadiabaticity in reaction waves as a mechanism for energy concentration. *Energy & Environmental Science* **7**, 3391–3402 (2014).

38. Ideally, the chemical potential gradient should also be just dependent on the fuel-thermal conduit pair and should remain constant as long as there is uniform reaction wave propagation. However factors such as non-uniform coating of fuel layer can lead to variable chemical potential gradient across samples. Also, this chemical potential gradient stops existing as soon as the reaction has completely propagated or has stopped after partial propagation. For partial propagation, we hypothesize that the charge carriers internally diffuse towards equilibration within the thermal conduit layer when the reaction wave has halted. Depending on the internal heat transfer properties of the system and the rate at which it loses heat to the surroundings, there is a possibility of reversal of the temperature gradient leading to opposite polarity voltage output contribution because of the thermoelectric effect. Interplay of factors such as the time dependence

Sustainable Power Sources Based on High Efficiency Thermopower Wave Devices

of the temperature gradient and the chemical potential gradient and practical conditions for device operation (e.g., non-adiabatic system and device-to-device differences) can explain the variety of types of voltage outputs.
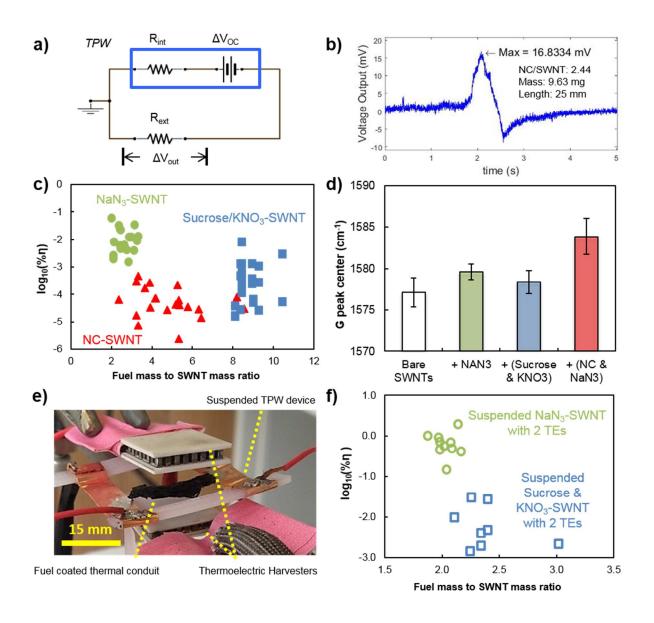

Figure 1 a) Circuit diagram for the electrical analysis of thermopower wave (TPW) devices where we connect an external load R_{ext} to measure the voltage drop ΔV_{out} across it. b) Sample of an actual thermopower wave voltage output. The voltage output for this 25 mm long reaction wave lasts for about 1.2 s. c) Chemical to electrical conversion efficiency of TPW devices using different fuels: Nitrocellulose (NC), Sodium azide and Sucrose with KNO_3. d) Doping analysis using Raman spectroscopy for different fueled and unfueled SWNT samples. The error bars represent 95% confidence intervals. e) A picture of an

Sustainable Power Sources Based on High Efficiency Thermopower Wave Devices

experimental setup involving TE harvesters (seen as white squares) suspended above and below a TPW device. f) Chemical to electrical conversion efficiencies of the updated TPW wave setups (i.e., including the electrical output from the reaction wave as well the TE harvesters).
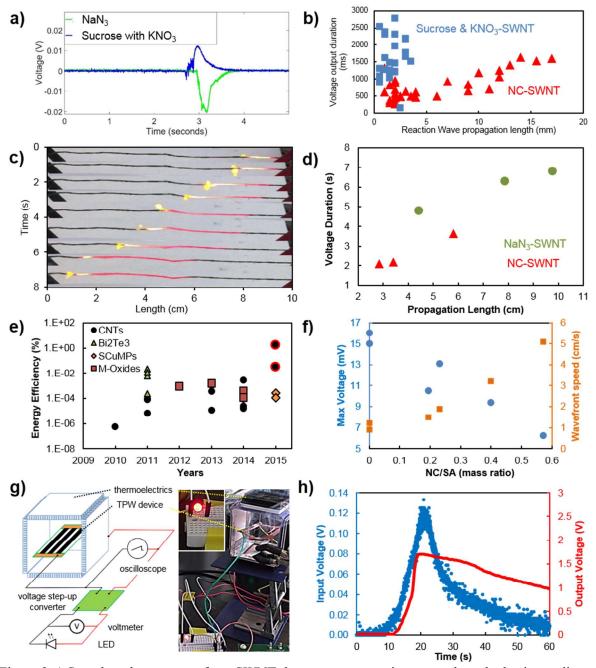

Figure 2 a) Sample voltage output from SWNT thermopower reaction waves launched using sodium azide and sucrose/KNO₃. b) Voltage output duration plotted against device length for nitrocellulose (NC) coated SWNTs and sucrose/KNO₃ coated SWNTs in the sub-centimeter regime. c) Time elapsed pictures displaying the reaction wave propagation on a 10 cm long NaN₃–SWNT TPW device. d) Decimeter-scale NaN₃ and nitrocellulose (NC) coated SWNTs showing linear scaling between voltage durations and wave

Sustainable Power Sources Based on High Efficiency Thermopower Wave Devices

propagation length. e) Master plot for chemical to electrical conversion efficiencies of all thermopower wave device setups published so far. The highest efficiency highlighted points in 2015 correspond to this work. f) Maximum voltage and speed of the reaction wavefront plotted against increasing nitrocellulose (NC) to sodium azide (SA) ratio. g) Schematic of the TPW-thermoelectric harvester setup coupled with a voltage step-up converter that illuminated a red LED (shown on the right) for 20 s. h) The input and output voltage measured across the step-up converter (a DC-to-DC power converter with an output voltage greater than its input voltage) plotted as a function of time. The LED stays on while the output voltage is above 1.5 V.
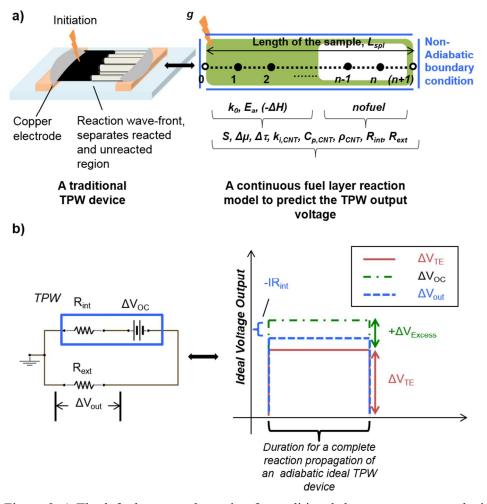

Figure 3 a) The left shows a schematic of a traditional thermopower wave device with a reaction wave propagation along a fuel coated thermal conduit connected to copper tape electrodes and supported on a glass slide. The right is a visualization of a model of a continuous layer of a fuel undergoing reaction to predict or fit the voltage output from a thermopower wave device. All of the properties (except the device's external heat loss properties) needed to completely define a thermopower wave device using such a scheme have been noted. b) The left shows a schematic of the electrical circuit diagram for analyzing the output voltage ΔV_{out} across an external resistor R_{ext} powered by a thermopower wave device with internal resistance R_{int}. The right shows an ideal voltage output profile for an adiabatic thermopower wave device undergoing complete reaction propagation. The open circuit voltage ΔV_{OC} from a

Sustainable Power Sources Based on High Efficiency Thermopower Wave Devices

thermopower wave device is contributed to by the temperature gradient and the chemical potential gradient.
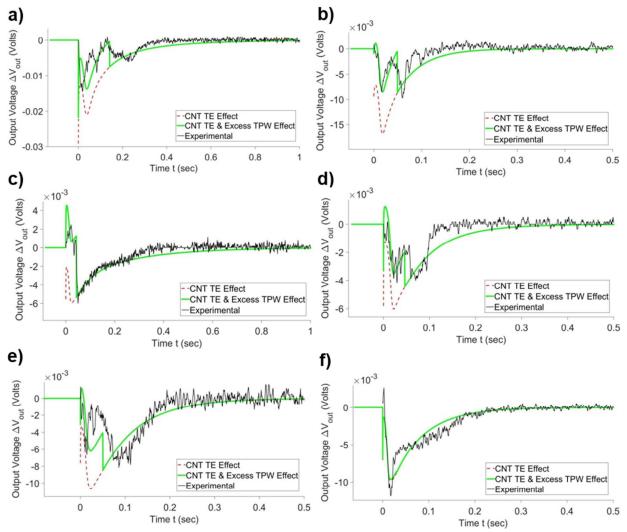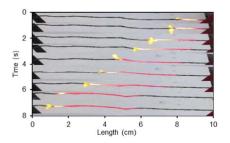

Figure 4 a-f) Thermopower wave voltage output prediction for experimental samples. The experimental output is shown in black, the model-predicted thermoelectric output is shown in red dotted lines, and the final model-predicted output is shown in green.

Table of contents entry

One sentence of text:

Thermopower wave devices are shown to achieve over 1% chemical-to-electrical conversion efficiency, producing energy densities on par with Li-ion batteries.

A brief paragraph (no more than 200 words) that puts the work into the broader context, highlighting the main advances and their impact on energy and environmental science.

Thermopower waves (TPWs) are self-propagating chemical reactions of a fuel along the length of a thermally and electrically conductive conduit. The reaction wave creates a corresponding voltage pulse of high specific power, that can potentially be used as a portable power source with extremely high power density. Quantum confined materials such as carbon nanotubes and graphene that have anisotropy in these transport properties are ideal for supporting such waves. In this work, we significantly enhanced the efficiency of electrical power generation using thermopower waves by designing fuels that interact favorably with the conduit and by harvesting the otherwise wasted convective heat from reaction. We show the scaling potential of such technology by fabricating a TPW device to an unprecedented length (10 cm), prolonging its energy generation, and for the first time, powering a commercial LED device. We further present a mathematical model of wave propagation that addresses both heat flow and electrical generation with energy losses to describe the observed experimental data. Specifically, the model explains why some waves produce one peak and others produce two opposite peaks in the transient voltage. Overall, this work demonstrates a substantial advance in the development of TPW portable, high power density sources.